




Research Article

PKN2 deficiency leads both to prenatal ‘congenital’ cardiomyopathy and defective angiotensin II stress responses

Jacqueline J.T. Marshall^{1,*}, Joshua J. Cull², Haged O. Alharbi², May Zaw Thin³, Susanna T.E. Cooper⁴, Christopher Barrington⁵, Hannah Vanyai^{6,†}, Thomas Snoeks⁷, Bernard Siow⁷, Alejandro Suárez-Bonnet^{8,9}, Eleanor Herbert^{8,9}, Daniel J. Stuckey³, Angus J.M. Cameron¹⁰, Fabrice Prin¹¹, Andrew C. Cook¹², Simon L. Priestnall^{8,9}, Sonia Chotani¹³, Owen J. L. Rackham¹³,  Daniel N. Meijles⁴, Tim Mohun¹¹,  Angela Clerk² and  Peter J. Parker^{1,14}

¹Protein Phosphorylation Laboratory, Francis Crick Institute, 1 Midland Road, London NW1 1AT, U.K.; ²School of Biological Sciences, University of Reading, Reading RG6 2AS, U.K.; ³UCL Centre for Advanced Biomedical Imaging, Division of Medicine, University College London, London WC1E 6DD, U.K.; ⁴Molecular and Clinical Sciences Institute, St George's University of London, London SW17 0RE, U.K.; ⁵Bioinformatics and Biostatistics, Francis Crick Institute, 1 Midland Road, London NW1 1AT, U.K.; ⁶Epithelial Biology Laboratory, Francis Crick Institute, 1 Midland Road, London NE1 1AT, U.K.; ⁷In Vivo Imaging, Francis Crick Institute, 1 Midland Road, London NW1 1AT, U.K.; ⁸Experimental Histopathology, Francis Crick Institute, 1 Midland Road, London NW1 1AT, U.K.; ⁹Department of Pathobiology & Population Sciences, The Royal Veterinary College, North Mymms, Hatfield, Hertfordshire AL9 7TA, U.K.; ¹⁰Kinase Biology Laboratory, John Vane Science Centre, Barts Cancer Institute, Queen Mary University of London, Charterhouse Square, London EC1M 6BQ, U.K.; ¹¹Heart Formation in Vertebrates Laboratory, Francis Crick Institute, 1 Midland Road, London NW1 1AT, U.K.; ¹²Centre for Morphology and Structural Heart Disease, Institute of Cardiovascular Science, Zayed Centre for Research, 20 Guilford Street, London WC1N 1DZ, U.K.; ¹³Program in Cardiovascular and Metabolic Disorders, Duke-NUS Medical School, Singapore, Singapore; ¹⁴School of Cancer and Pharmaceutical Sciences, New Hunt's House, Guy's Campus, London SE1 1UL, U.K.

Correspondence: Peter J. Parker (peter.parker@crick.ac.uk) or Angela Clerk (a.clerk@reading.ac.uk)



The protein kinase PKN2 is required for embryonic development and PKN2 knockout mice die as a result of failure in the expansion of mesoderm, cardiac development and neural tube closure. In the adult, cardiomyocyte PKN2 and PKN1 (in combination) are required for cardiac adaptation to pressure-overload. The specific role of PKN2 in contractile cardiomyocytes during development and its role in the adult heart remain to be fully established. We used mice with cardiomyocyte-directed knockout of PKN2 or global PKN2 haploinsufficiency to assess cardiac development and function using high resolution episcopic microscopy, MRI, micro-CT and echocardiography. Biochemical and histological changes were also assessed. Cardiomyocyte-directed PKN2 knockout embryos displayed striking abnormalities in the compact myocardium, with frequent myocardial clefts and diverticula, ventricular septal defects and abnormal heart shape. The sub-Mendelian homozygous knockout survivors developed cardiac failure. RNASeq data showed up-regulation of PKN2 in patients with dilated cardiomyopathy, suggesting an involvement in adult heart disease. Given the rarity of homozygous survivors with cardiomyocyte-specific deletion of PKN2, the requirement for PKN2 in adult mice was explored using the constitutive heterozygous PKN2 knockout. Cardiac hypertrophy resulting from hypertension induced by angiotensin II was reduced in these haploinsufficient PKN2 mice relative to wild-type littermates, with suppression of cardiomyocyte hypertrophy and cardiac fibrosis. It is concluded that cardiomyocyte PKN2 is essential for heart development and the formation of compact myocardium and is also required for cardiac hypertrophy in hypertension. Thus, PKN signalling may offer therapeutic options for managing congenital and adult heart diseases.

*Current address: Cancer Research UK, 2 Redman Place, London E20 1JQ, U.K.

†Current address: The Walter and Eliza Hall Institute, 1G Royal Parade, Parkville, 3052, Australia

Received: 30 May 2022
Revised: 21 June 2022
Accepted: 21 June 2022

Accepted Manuscript online:
22 June 2022
Version of Record published:
12 July 2022

Introduction

Heart disease, a major cause of death and disability worldwide, develops from numerous underlying causes. These include genetic/environmental interactions causing congenital cardiac defects [1, 2], in addition to diseases in later life resulting from various pathophysiological stressors (e.g. coronary artery disease, hypertension, diabetes, obesity) [3–8]. The increasing prevalence of heart disease worldwide accounts for an expanding patient cohort who go on to develop and die of heart failure. The heart contains three main cell types (cardiomyocytes, endothelial cells, fibroblasts) with cardiomyocytes providing the contractile force. In the embryo/foetus, cardiomyocytes proliferate whilst the heart develops, but then withdraw from the cell cycle in the perinatal/postnatal period, becoming binucleated and fully terminally differentiated [9, 10]. Further growth of the heart to the adult size requires an increase in size and sarcomeric/myofibrillar apparatus of individual cardiomyocytes (maturation growth). The adult heart experiences pathophysiological stresses (e.g. hypertension) requiring an increase in contractile function. This is accommodated by cardiomyocyte hypertrophy (sarcomeric replication in parallel or series) with associated cardiac hypertrophy (enlargement of the heart) [11]. This adaptation is initially beneficial, but pathological hypertrophy develops over prolonged periods with cardiomyocyte dysfunction and death, loss of capillaries and deposition of inelastic fibrotic scar tissue [11]. These processes are all regulated by a complex interplay of intracellular signalling pathways, driven by numerous protein kinases that play central roles both in mammalian development and in adult tissue homeostasis [12]. These regulatory proteins offer themselves as potential targets for intervention both in management of congenital cardiomyopathies and in pathological states. Insight into the key regulatory players at each and every stage is central for prevention, in addition to the development and delivery of improved treatments and outcomes.

The Protein Kinase N (PKN) family of kinases are emerging as potential therapeutic targets for heart disease [13]. Whilst PKN1 and PKN2 are ubiquitously expressed in tissues throughout the body, PKN3 is expressed in a smaller subset of tissues, especially endothelial cell types [14, 15]. Of the three PKNs, only *Pkn2* knockout is embryonic lethal. This is due to failure in the expansion of mesoderm tissues, failure of cardiac development and compromised neural tube closure [16, 17]. Further studies with conditional knockouts of *Pkn2* employed cell-targeted Cre under the control of a smooth muscle protein 22 α (SM22 α) promoter [17]. SM22 α (and therefore SM22 α -Cre) is expressed in the heart tube from embryonic day E7.5/8 [18], with expression declining from E10.5 and becoming restricted to the right ventricle by E12.5. By E13.5, SM22 α is undetectable in the heart [19] and expression is subsequently confined to smooth muscle cells and myofibroblasts [18, 20–22]. Conditional gene deletion of *Pkn2* results in sub-Mendelian survival of SM22 α -Cre^{+/-} *Pkn2*^{fl/fl} offspring, with ~1/3 of mice surviving to 4 weeks postnatally [17]. These data indicate that PKN2 is not only important in the heart during embryonic development, but (whilst the phenotype is not fully penetrant in the SM22 α -Cre model) is also required for maturational growth of the heart. This raises the question of what is compromised and how loss of PKN2 manifests in the adult.

There are few studies of PKNs in the adult heart. PKN1 is activated in neonatal cardiomyocytes by hyperosmotic shock [23] and reduces ischaemia/reperfusion injury in *ex vivo* perfused hearts [24]. *In vivo* studies suggest there may be redundancy between PKN1 and PKN2 in cardiomyocytes, and double knockout of both kinases simultaneously in cardiomyocytes inhibits cardiac hypertrophy in pressure-overload conditions induced by transverse aortic constriction (TAC) or angiotensin II (AngII) [25]. Fundamental questions remain concerning the functional redundancy of PKN1 and 2 in cardiomyocytes. Here, we demonstrate that the loss of PKN2 in cardiomyocytes has a catastrophic effect on ventricular myocardial development, suggesting that alterations in PKN2 signalling may contribute to congenital cardiac problems/cardiomyopathy. We also demonstrate that PKN2 haploinsufficiency compromises cardiac adaptation to hypertension in adult mouse hearts. We conclude that PKN2 plays a significant and non-redundant role in cardiac development and adaptation.

Results

Cardiac-specific knockout of *Pkn2*

Evidence from the SM22 α -Cre conditional *Pkn2* knockout indicates reduced survival (Table 1 and [17]), which might reflect in part an impact on heart function but may also be determined by loss of *Pkn2* expression in smooth muscle. To dissect the functional contributions more selectively, we sought to refine the pattern of knockout by using the XMLC-Cre line, where Cre expression is cardiac restricted [26]. Genotyping pups from the *Pkn2*^{fl/fl} mice crossed with XMLC2-Cre^{+/-} *Pkn2*^{fl/+} animals at 2–4 weeks of age identified only one XMLC2-Cre^{+/-} *Pkn2*^{fl/fl} mouse (of 126), consistent with a severe phenotype with this Cre line (Table 1). This potentially results from higher efficiency of XMLC2-Cre activity in cardiomyocytes (95% [26]) compared with

Table 1 *SM22αCre* and *XMLC2Cre* mouse strain crosses are indicated in column 1, with numbers of experimentally determined genotypes shown in rows for the age ranges defined

Parent genotypes	Age	Cre negative		Cre positive		Fisher's test	Representation
		PKN2 ^{fl/+}	PKN2 ^{fl/fl}	PKN2 ^{fl/+}	PKN2 ^{fl/fl}		
SM22α-Cre ^{+/-} -PKN2 ^{fl/+} × PKN2 ^{fl/fl}	E14.5–E18.5	54	43	33	46	>0.5	Mendelian under-represented
	3 weeks	166	215	176	44	0.0001	
XMLC2-Cre ^{+/-} -PKN2 ^{fl/+} × PKN2 ^{fl/fl}	E14.5–E18.5	5	3	10	6	>0.5	Mendelian under-represented
	3 weeks	37	41	47	1	0.0001	

The representation of the PKN2 knockout (i.e. PKN2^{fl/fl} in the context of Cre expression) was analysed as a function of the all genotypes using Fisher's test.

SM22α-Cre (75–80% [20]) and more specifically indicates that there are cardiac-associated phenotypes of PKN2 loss. The single surviving male was small (11.2 g relative to 22.4 g for a *XMLC2-Cre^{+/-} Pkn2^{fl/+}* littermate) and was culled at 5 weeks due to poor condition. Histological analysis of the heart from this animal showed that it was highly abnormal. Both ventricles were dilated, with a hypertrophic right ventricle and thin-walled (hypotrophic) and disorganised left ventricular myocardium and interventricular septum. There were partial discontinuities in the cardiac muscle of the compact layer, and sections with highly disorganised cardiomyocytes and fibrosis (Figure 1a). It was noted also that the lungs from the *XMLC2-Cre^{+/-} Pkn2^{fl/fl}* mouse displayed grossly enlarged alveolar spaces (Figure 1b).

To explore this impact of PKN2 further, we genotyped gestational day 14.5 embryos from *Pkn2^{fl/fl}* mice crossed with *XMLC2-Cre^{+/-} Pkn2^{fl/+}* and found that 6 of 24 were *XMLC2-Cre^{+/-} Pkn2^{fl/fl}* consistent with a Mendelian distribution at this developmental stage. However, analysis of the hearts using high resolution episcopic microscopy (HREM) showed various abnormalities (Figure 1c; Video 1 see also Supplementary Figure S1). Notably, hearts from these mouse embryos displayed multiple surface nodules (diverticula; see below) distributed across both ventricles, unusually large perimembranous ventricular septal defects and thin compact myocardium indicative of significant cardiac developmental complications.

Characterising the cardiac requirement of PKN2

Whilst the *XMLC*-driven knockout of *Pkn2* clearly demonstrated a cardiac phenotype associated with PKN2 loss, the fatal consequences of the *XMLC*-driven knockout of *Pkn2* led us instead to investigate in more detail the more frequent survivors derived in the *SM22α-Cre* model. On re-derivation of the *SM22α* model into a new facility and crossing the *Pkn2^{fl/fl}* with *SM22α-Cre^{+/-} Pkn2^{fl/+}* animals, we found there remained a sub-Mendelian distribution of the *SM22α-Cre^{+/-} Pkn2^{fl/fl}* genotype (28% of expected numbers with no male/female bias; Table 1). Crossing 10 of these mice with *Pkn2^{fl/fl}* animals produced 62 weaned pups but again a sub-Mendelian representation of the *SM22α-Cre^{+/-} Pkn2^{fl/fl}* genotype (32% of expected).

Typically, surviving *SM22α-Cre^{+/-} Pkn2^{fl/fl}* mice became overtly unwell as they aged, displaying a range of adverse phenotypes including body weight differences compared with littermates, loss of condition, hunched appearance or reduced activity. Amongst a cohort of 23 animals, there were 50% asymptomatic *SM22α-Cre^{+/-} Pkn2^{fl/fl}* mice at 24 weeks of age, with the oldest two mice reaching 72 weeks and only then started to display phenotypes (echocardiography showed aortic valve stenosis and echo-dropout across the long-axis view of the left ventricle in one, suggestive of mitral annular calcification; see below). A typical example of an aging *SM22α-Cre^{+/-} Pkn2^{fl/fl}* animal was a 38-week-old fertile female which upon culling due to loss of condition displayed a heart weight: body weight ratio = 0.99% (compared with 0.37–0.48% for female littermates).

Similar to the single weaned *XMLC2-Cre^{+/-} Pkn2^{fl/fl}* mouse, histology of the *SM22α-Cre^{+/-} Pkn2^{fl/fl}* mice showed hypertrophic ventricular walls with disorganised cardiomyocytes and extensive fibrosis, consistent with a form of cardiomyopathy and heart failure (Figure 2a,b; Supplementary Figure S2). Histological assessment of the lungs showed *SM22α-Cre^{+/-} Pkn2^{fl/fl}* mice culled with breathlessness had grossly enlarged alveolar spaces (Figure 2c), corresponding to the anecdotal finding in the one *XMLC-Cre^{+/-} Pkn2^{fl/fl}* survivor. The timing of symptom onset is illustrated in Figure 2d. Functional cardiac MRI analysis of a further set of five surviving *SM22α-Cre^{+/-} Pkn2^{fl/fl}* mice with initial symptoms of heart failure, indicated that they had reduced left ventricular ejection fraction (Figure 2e,f). Imaging did not identify a single unifying cause, with examples of

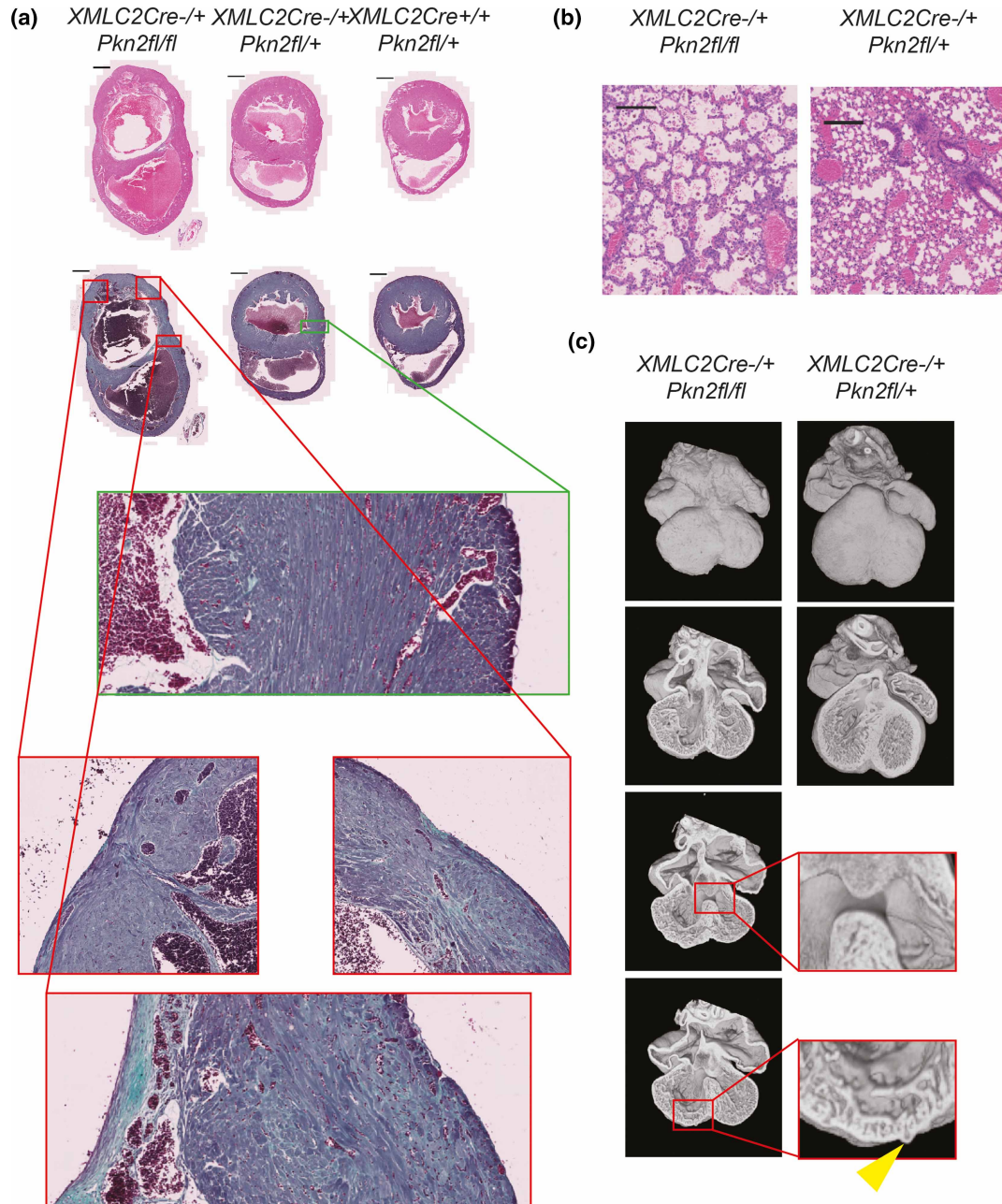


Figure 1. PKN2 knockout in cardiomyocytes causes defective embryonic heart development leading to failure prior to adulthood.

(a) H&E and Gomori's Trichrome stained histological cardiac short-axis sections of the longest surviving *XMLC2Cre^{+/-} Pkn2^{fl/fl}* genotype mouse (left; male), and two littermates (middle & right; male *XMLC2Cre^{+/-} Pkn2^{fl/+}* & female *XMLC2Cre^{+/-} Pkn2^{fl/+}*, respectively) all culled aged 5 weeks. Scale bars are 1 mm. In lower boxed regions, various sections are also shown at 20× zoom relative to whole-heart cross-sections. (b) H&E sections of lungs of the same *XMLC2Cre^{+/-} Pkn2^{fl/fl}* genotype mouse (left), and its *XMLC2Cre^{+/-} Pkn2^{fl/+}* littermate (right; both male). Scale bars are 200 μm. (c) Images of High-Resolution Episcopic Microscopy (HREM) reconstructions of E14.5 embryo hearts for the genotypes indicated, showing surface and four chamber views. Boxed regions of sections are shown at 4× zoom; a diverticulum is indicated by the yellow arrowhead.

reduced right ventricular mass, potentially associated with pulmonary hypertension ($n = 2$ of 5), or completely abnormal architecture with hearts exhibiting a bulbous shape ($n = 3$ of 5) (see histology and HREM in Supplementary Figures S2 and S3).

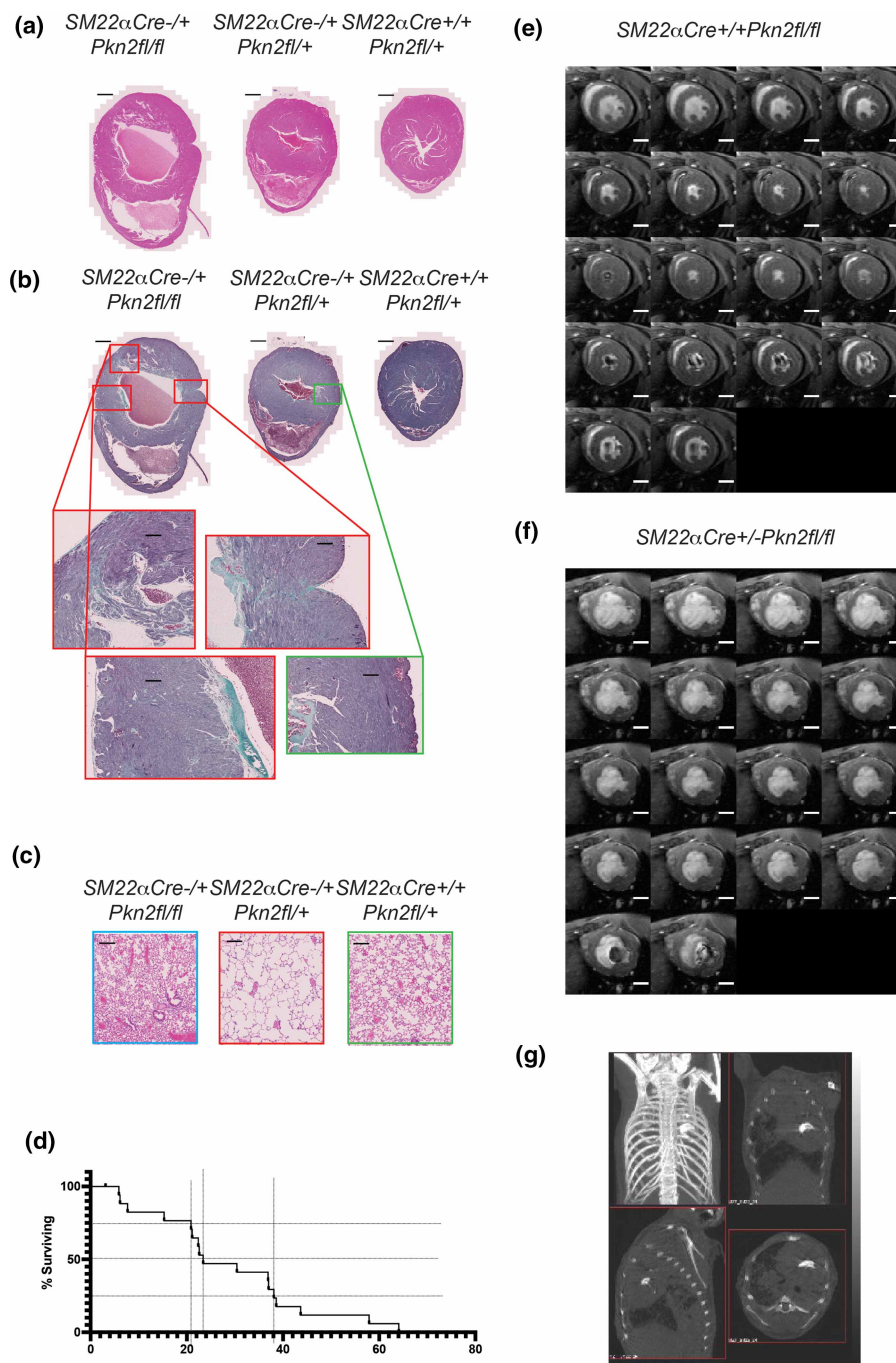


Figure 2. *SM22αCre^{+/-} Pkn2^{fl/+}* mice suffer cardiac failure on aging.

(a and b) Short-axis mid-ventricle sections of hearts of 39 week male littermates of the genotypes indicated, stained with H&E (a), or Gomori's Trichrome (b). (c) H&E stained sections of lungs, littermates as in (a and b). (d) Time course of symptom onset for mice of genotype *SM22αCre^{+/-} Pkn2^{fl/fl}* ($n = 23$). (e and f) Montage of time-series through the cardiac cycle recorded by cine-cardiac-MRI through the short-axis plane at mid-ventricle from *SM22αCre^{+/+} Pkn2^{fl/fl}* (e) and *SM22αCre^{+/-} Pkn2^{fl/fl}* (f) 32 week old female littermates. (g) micro-CT of the thorax of a 24 week *SM22αCre^{+/-} Pkn2^{fl/fl}* female shown as a projected image and slice images in three planes. Scale-bars in histopathology images are 1 mm in whole heart sections (panels a and b) and 200 μm in zoomed sections (panels b and c). Scale-bars in MRI montages are 2 mm (panels e and f).

Micro-CT imaging was used to assess disease in a further subset of survivors. This revealed variously: pulmonary oedema and pleural effusion, and marked, unusual calcification in the centre of the rib cage (Figure 2g). Subsequent micro-CT of fixed hearts showed that calcification appeared to be associated with both the aortic and mitral valves (Supplementary Video S2). The evidence suggests that surviving *SM22α-Cre^{+/-} Pkn2^{fl/fl}* mice had congenital defects in the heart and/or lungs resulting in heart failure and as with human congenital heart disease, there was heterogeneity with respect to age of disease onset, severity of disease and specific cardiac phenotype.

Cardiomyocyte PKN2 is essential for normal cardiac development

Although previous studies reported that PKN2 is essential for embryonic development, E13.5 embryos were produced at a normal Mendelian ratio [17]. Data from surviving *SM22α-Cre^{+/-} Pkn2^{fl/fl}* mice (above) suggest the cardiac defect is most likely the result of developmental cardiac abnormalities, however defects in lung development resulting from loss of Pkn2 in smooth muscle cells would impact cardiac function and also lead to heart failure. We therefore collected embryos at E14.5–E18.5 generated by crossing *Pkn2^{fl/fl}* and *SM22α-Cre^{+/-} Pkn2^{fl/+}* mice for further analysis to examine the Mendelian ratios at these later embryonic stages, and to enable pathological examination of the developing hearts and lungs. Genotype distribution was Mendelian at both E14.5 and E18.5 (Table 1). Notably, histological analysis failed to identify any difference between lungs from *SM22α-Cre^{+/-} Pkn2^{fl/fl}* embryos and those from littermates that were either *Cre* negative or heterozygous for the floxed *Pkn2* allele or both (Figure 3a), suggesting normal lung development to E18.5 and implying that the enlarged alveolar spaces in some of the rare surviving adults may be a secondary consequence of cardiac abnormalities.

Given that the E18.5 genotype distribution was Mendelian but only ~30% of *SM22α-Cre^{+/-} Pkn2^{fl/fl}* mice survived to weaning, this suggested that lethality occurred in the perinatal period. Analysis of deceased pups including part-cannibalised carcasses demonstrated that this genotype was selectively lost in this very early neonatal stage (Table 1). Veterinary pathologist characterisation of P1.5–P5.5 carcasses showed that all had normal palates, lungs that floated and milk spots. There were no observations of pericardial bleeding, which might have been observed if one of the cardiac diverticula had ruptured causing tamponade (see below).

Analysis of embryo hearts using HREM showed that of 16 *SM22α-Cre^{+/-} Pkn2^{fl/fl}* E14.5 embryos, 15 had overt defects in cardiac development compared with littermates (exemplified in Figure 3b; see also Supplementary Figure S3). Defects included perimembranous ventricular septal defects (pVSDs), small muscular VSDs (mVSDs), thin compact myocardium (right and left ventricle) and overt nodules on the external surface of either or both ventricles. The degree of phenotype varied, with the most abnormal hearts showing pVSD with overriding of the aorta (OA), and many showing an overall abnormally squat shape with an indistinct apex. The nodules on the surface of the ventricles were examined histologically and identified as diverticula with internal lumens connected to the ventricular cavities (Figure 3c).

Cardiac septation would expect to be completed by E15, however of 60 embryos analysed in crosses of *Pkn2^{fl/fl}* and *SM22α-Cre^{+/-} Pkn2^{fl/+}* mice, we obtained 18 *SM22α-Cre^{+/-} Pkn2^{fl/fl}* embryos of which seven had persistent VSDs along with thin compact myocardium/ventricular walls. The nodules on the ventricle surfaces apparent at E14.5 also persisted. There was additional abnormal development of the trabecular layer in the ventricular walls — analogous to hypertrabeculation (Figure 3d).

The congruence of developmental defects in the *SM22α-Cre* and the *XMLC-Cre* strains indicates that the dominant effect of tissue-specific *Pkn2* loss relates to the shared aspect between these models, namely an impact on cardiomyocytes rather than, for example any later embryonic stage stromal loss of *Pkn2*. Although there is the potential for additional influences of the *SM22α-Cre Pkn2* knockout model via vascular smooth muscle, this is unlikely to have any profound impact given the phenotype of the *XMLC-Cre* strain is more penetrant not less so. It is surmised that this reflects the higher efficiency of this latter promoter in cardiomyocytes [26]. These observations of developmental abnormalities in the heart are consistent with the conclusion that the failure of these *Cre^{+/-} Pkn2^{fl/fl}* mice to thrive, and in particular the cardiac abnormalities in the rare survivors, reflect congenital problems. The rarity of these survivors and the legacy of the developmental defects compromise the assessment of the role of PKN2 in adults in these models and alternative strategies are required.

Expression of PKN2 in the adult heart

Pkn2 is expressed in adult cardiomyocytes [12]. Although expression levels relative to total protein decline during postnatal development, this is because cardiomyocyte size increases substantially, and the relative

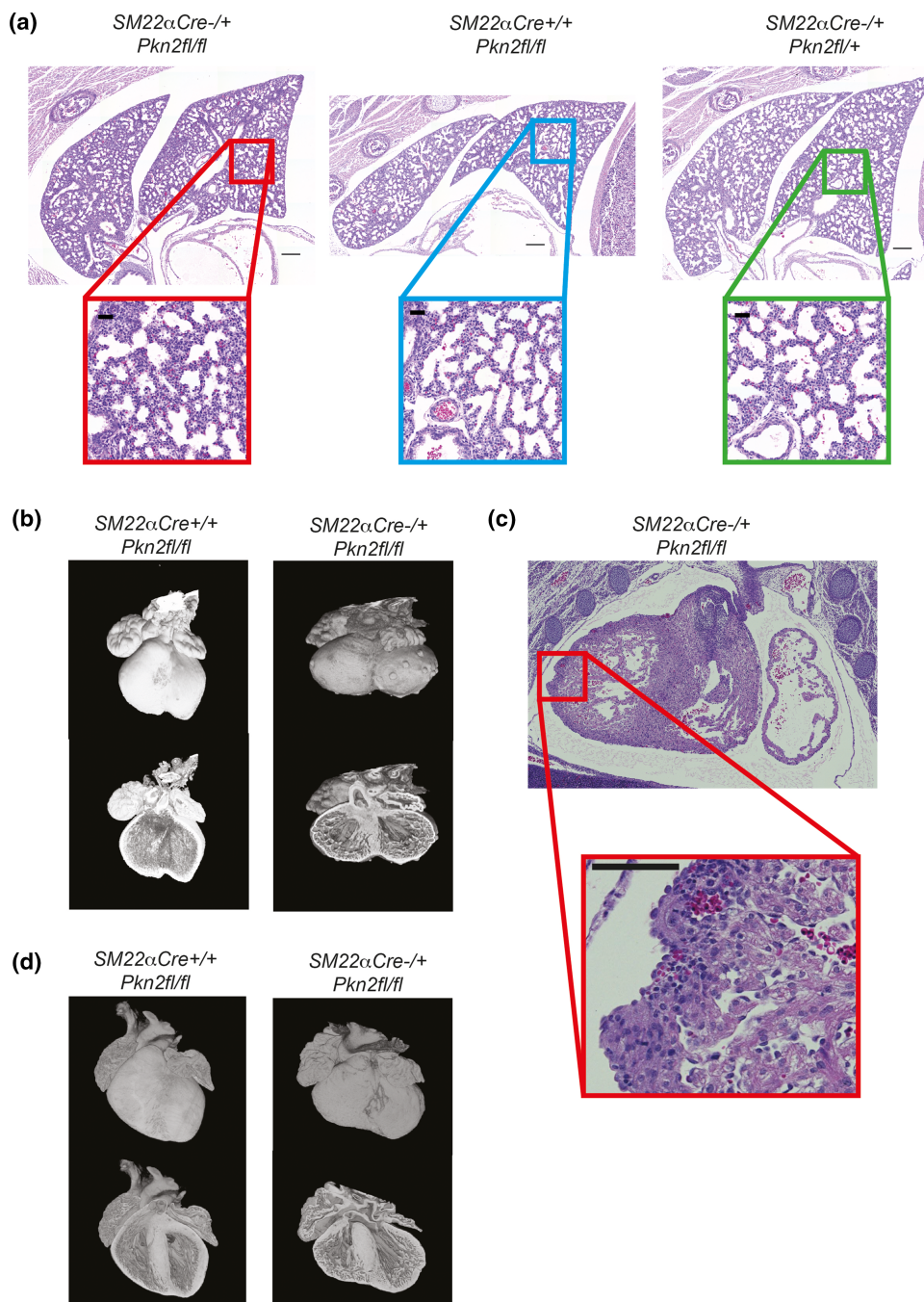


Figure 3. The heart-specific defects in *SM22αCre^{+/-}Pkn2^{fl/fl}* mice.

(a) H&E stained sections of (E18.5) lungs of littermates with the indicated genotypes. Lower boxed panels are 5× zoomed; scale bars indicate 200 μm in upper panels and 40 μm in lower zoomed panels. (b) Reconstructions of E14.5 hearts imaged by HREM are shown in surface (top images) and slice (lower images) views. The genotypes are as indicated. (c) H&E stained E14.5 heart sections featuring an outer ventricular surface nodule, identified as a diverticulum. Scale bars are 100 μm. (d) Reconstructions of E18.5 hearts imaged by HREM shown as per panel (b). Genotypes are as indicated.

amount of PKN2 per cell increases in the adult (Supplementary Figure S4). To determine if variations in *PKN2* expression may be associated with human heart failure, we mined an RNASeq database of patients with dilated cardiomyopathy ($n = 97$) vs normal controls ($n = 108$) [27]. All PKN isoforms were detected in human hearts,

but *PKN2* expression increased in dilated cardiomyopathy (DCM) hearts relative to controls, whilst *PKN1* and *PKN3* declined (Figure 4a). To determine if PKN2 may be involved in disease aetiology, we assessed expression in a mouse model of hypertension induced by angiotensin II (AngII; 0.8 mg/kg/d, 7 days). Expression of PKN2, but not PKN1, increased with AngII treatment relative to vehicle-treated controls (Figure 4b). This suggests that altered expression may contribute to the adaptive response to hypertension and/or may be associated with progression towards a pathological state. To assess whether altered expression might impact this response and in view of the impact of *Pkn2* knockout as described above, we focused on the effects of haploinsufficiency (global loss of a single allele, i.e. *Pkn2*Het mice). PKN2 protein expression was reduced in hearts from male *Pkn2*Het mice relative to WT littermates (Figure 4c). There was no compensatory increase in PKN1 expression although the relative level of phosphorylation of PKN2 was increased. *Pkn2*Het mice thus provide a model for assessment of altered expression in the adult heart.

The role of PKN2 in the adult heart

We assessed the baseline dimensions and function of the hearts from *Pkn2*Het mice and WT littermates using echocardiography (Figure 4d,e; Supplementary Table S1). M-mode imaging of the short-axis view revealed that *Pkn2*Het mice had a small but significant reduction in left ventricle (LV) wall thickness compared with WT littermates. Assessment of cardiac function using speckle-tracking strain analysis confirmed that overall LV mass was significantly decreased in *Pkn2*Het mice and there was a small, albeit non-significant, increase in ejection fraction (Figure 4e; Supplementary Table S1). We conclude that there are abnormalities in surviving *Pkn2*Het mice and, although these changes appear relatively minor, they may compromise cardiac adaptation to pathophysiological stresses such as hypertension.

To determine if the hearts from *Pkn2*Het mice can adapt to hypertension, adult male *Pkn2*Het mice or WT littermates (aged 11–14 weeks) were treated with AngII or vehicle for 7 d and cardiac dimensions/function were assessed by echocardiography (Figure 4f–h; Supplementary Table S2). As in previous studies [28, 29], AngII promoted cardiac hypertrophy in WT mice, with decreased LV internal diameter and significantly increased LV wall thickness (Figure 4f,h). AngII promoted similar changes in *Pkn2*Het mice, although ventricular wall thickening appeared reduced with no significant difference relative to vehicle-treated mice (Figure 4h). Strain analysis of B-mode images confirmed that the increase in LV mass induced by AngII was attenuated in *Pkn2*Het mice (Figure 4g,h). In addition, AngII significantly increased ejection fraction and fractional shortening in WT mice, but not *Pkn2*Het mice, indicating that cardiac adaptation to hypertension in response to AngII was attenuated. Histological staining showed that AngII increased cardiomyocyte cross-sectional area in WT mice, but not in *Pkn2*Het mice (Figure 5a). AngII increased cardiac fibrosis in interstitial areas of the myocardium, particularly at the junctions between the outer LV wall and the interventricular septum, but this was similar in both WT and *Pkn2*Het mice (Figure 5b). AngII also increased fibrosis in the perivascular regions of arteries/arterioles, and this was reduced in *Pkn2*Het hearts compared with hearts from WT mice (Figure 5c). Overall, cardiac adaptation to hypertension was reduced in *Pkn2*Het mice compared with WT littermates, with both reduced cardiomyocyte hypertrophy and perivascular fibrosis.

To gain mechanistic insight into the effects of PKN2 in the cardiac response to hypertension, we used RNASeq to assess the transcriptional differences in the AngII response of hearts from *Pkn2*Het mice compared with WT littermates (Figure 5d). No differentially expressed genes (DEGs) were identified when comparing *Pkn2*Het and WT hearts from mice treated with either vehicle or AngII. AngII-treatment resulted in 2272 DEGs in hearts from WT or *Pkn2*Het mice ($P < 0.01$): 699 were identified in both genotypes, 1371 were only detected in WT hearts and 202 were only detected in *Pkn2*Het hearts (Figure 5d(i), Supplementary Tables S3–S8). Clustering the DEGs according to function highlighted significant changes in a subset of genes for the myofibrillar apparatus and cytoskeletal structures, particularly the actin cytoskeleton, but there were no overall differences between the genotypes/treatment in these gene classes as a whole (Figure 5d(ii)). In contrast, genes associated with fibrosis were significantly up-regulated by AngII (Figure 5d(iii)), particularly those associated with collagen production (Figure 5d(iv)). The response in hearts from *Pkn2*Het mice was reduced relative to WT littermates, consistent with a reduction in perivascular fibrosis seen by histology (Figure 5c). Another notable feature of the AngII response was the reduction in the expression of genes for mitochondrial proteins (Figure 5d(v)). The overall response was reduced in *Pkn2*Het mice, but the effect was more pronounced for some genes, particularly those of the tricarboxylic acid (TCA) cycle (Figure 5d(vi)). AngII cardiac hypertrophy is associated with inflammation and we detected a clear interferon response (Figure 5d(vii)) with up-regulation of the complement pathway (Figure 5d(viii)). Both of these responses were reduced in hearts from *Pkn2*Het

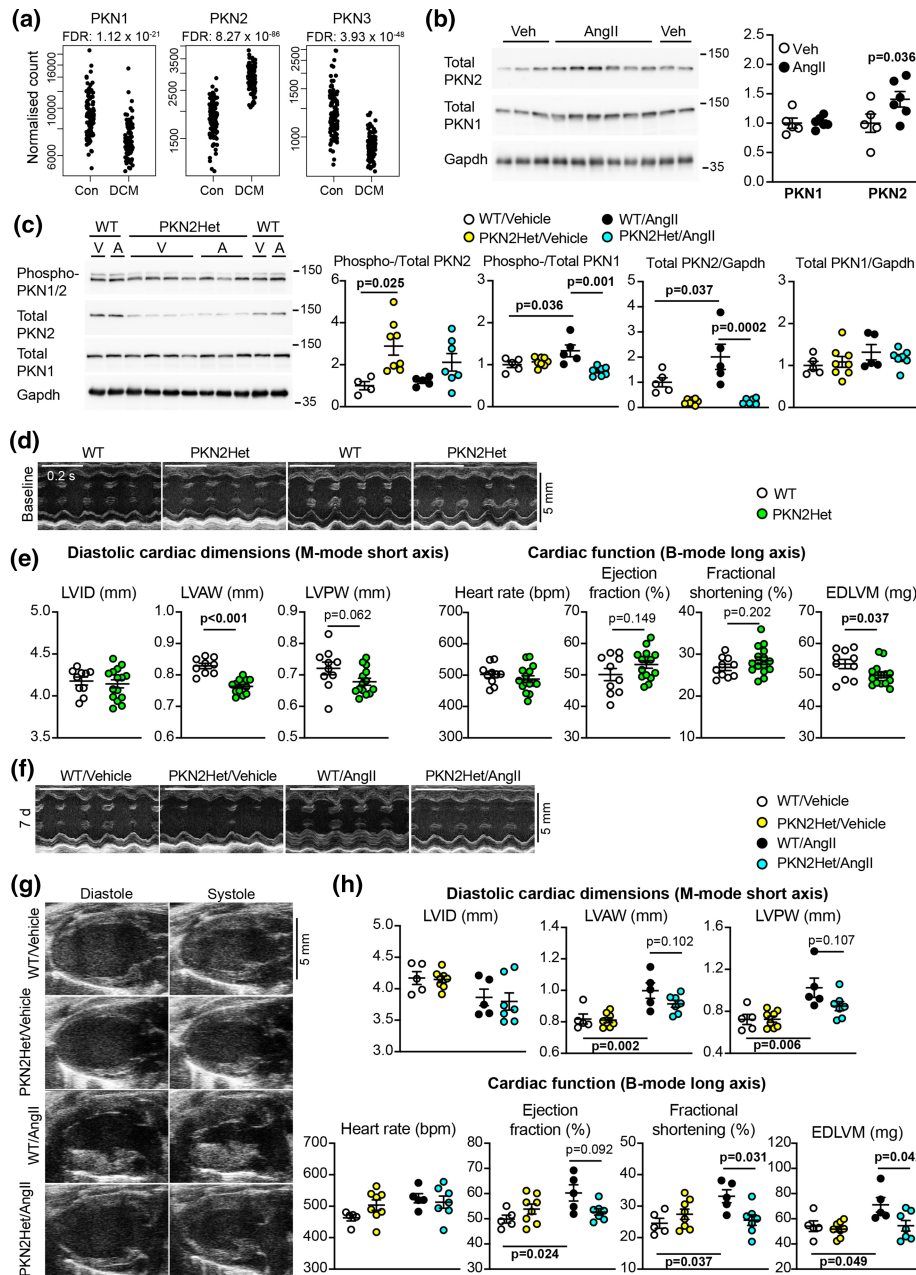


Figure 4. PKN2 is associated with human heart failure and required for cardiac adaptation to hypertension in mice.

(a), Expression of *PKN1*, *PKN2* and *PKN3* in human hearts. Data were mined from an RNASeq database of patients with dilated cardiomyopathy (DCM; $n = 97$) and normal controls (Con; $n = 108$). Data for individual samples are shown with false discovery rates (FDR). (b and c) Immunoblotting of phospho-PKN1/2, total PKN1, total PKN2 and GAPDH in hearts from wild-type (WT) or *Pkn2*Het mice treated for 7 days with vehicle (Veh, V) or 0.8 mg/kg/d angiotensin II (AngII, A). Immunoblots are shown on the left with densitometric analysis on the right (normalised to the mean of vehicle-treated controls). Individual data points are provided with means \pm SEM. Analysis used two-way ANOVA with Holm–Sidak’s post-test. (d–h), Echocardiography of hearts from WT and *Pkn2*Het mice at baseline (d and e) or treated with vehicle or AngII for 7 days (f–h). Representative short-axis M-mode images used for assessment of cardiac dimensions are shown at baseline (d) and after treatment (f) (the same animals are shown). (g), Representative long-axis B-mode images used for speckle-tracking and strain analysis to assess cardiac function are shown after 7 days treatment. (e and h), Echocardiograms were analysed. Individual data points are provided with means \pm SEM. Additional data are provided in Supplementary Table S1 and histology in S2. Analysis used unpaired, two-tailed *t*-tests (e) or two-way ANOVA with Holm–Sidak’s post-test (g). LV, Left ventricle; ID, internal diameter; AW, anterior wall; PW, posterior wall; EDLVM, end diastolic LV mass.

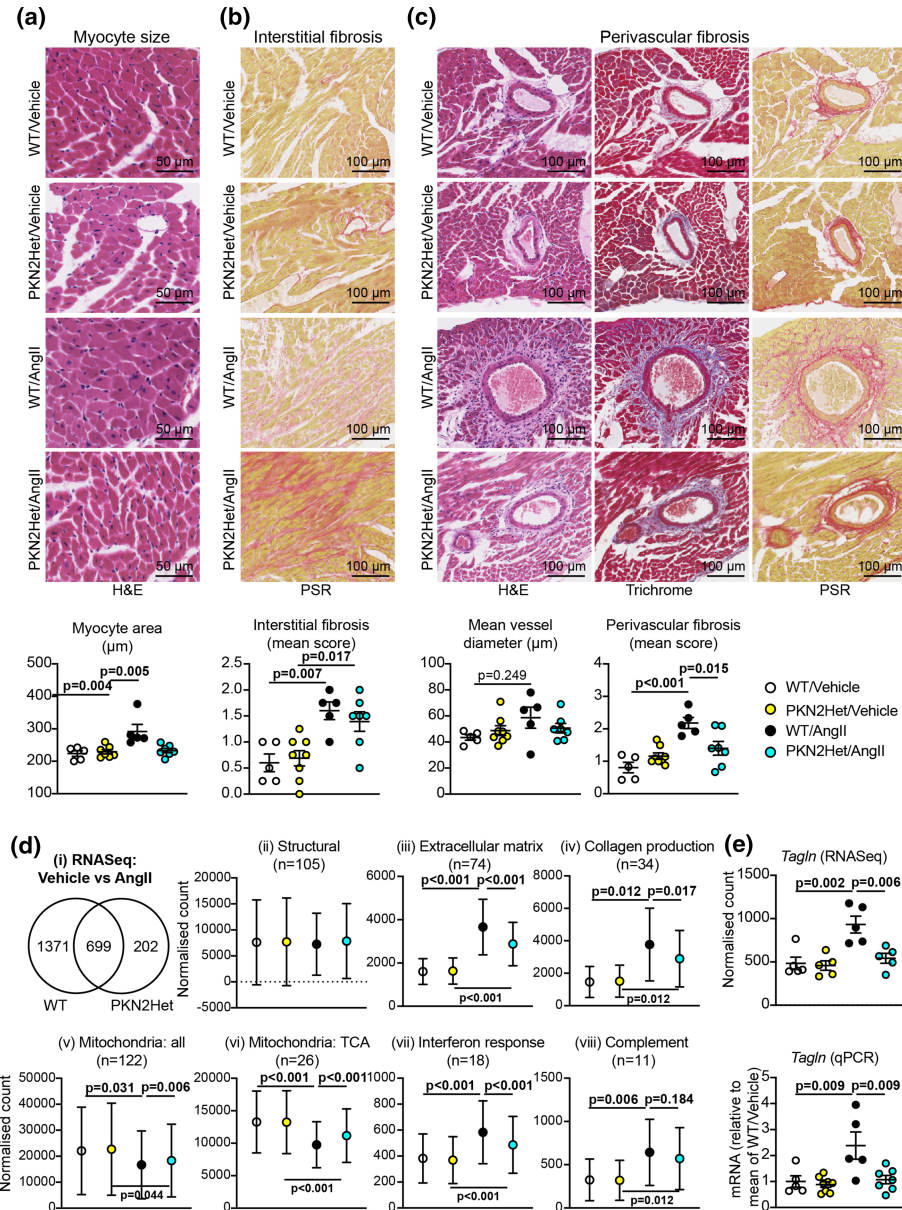


Figure 5. *Pkn2* haploinsufficiency reduces cardiac adaptation to hypertension, affecting cardiomyocyte size, perivascular fibrosis and gene expression.

WT or *Pkn2*Het mice were treated with vehicle or AngII (0.8 mg/kg/d) for 7 days. (a–c), Sections of WT and *Pkn2*Het mouse hearts were stained with haematoxylin and eosin (H&E), picosirius red (PSR), or Masson’s Trichrome. Representative images are shown with quantification provided below. Individual data points are provided with means \pm SEM. Analysis used two-way ANOVA with Holm–Sidak’s post-test. (d), RNASEq analysis of hearts from WT and *Pkn2*Het mice. (i) Summary of differentially-expressed genes ($P < 0.01$ resulting from AngII treatment. (ii)–(viii) Clusters of DEGs according to function. Results are the mean normalised count values with 95% CI for the n values indicated. Analysis used one-way ANOVA with Holm–Sidak’s post-test. (e) Comparison of *Tagln* (SM22 α) mRNA expression assessed by RNASEq and qPCR. Individual data points are shown with means \pm SEM. Analysis used two-way ANOVA with Holm–Sidak’s post-test.

mice relative to WT littermates. Data for individual genes in each of the clusters are in Supplementary Table S9. We mined the data for classical markers of cardiac hypertrophy and detected increased expression of *Myh7*, *Nppa* and *Nppb* with AngII as expected [11], but expression was similar in *Pkn2*Het and WT mice (Supplementary Figure S5). We also detected up-regulation of *Tagln* (SM22 α) by AngII in WT, but not

*Pkn2*Het mouse hearts (Figure 5e). *SM22α* is a marker of smooth muscle cells in the adult, and this is potentially a reflection of the perivascular fibrosis induced by AngII around arteries/arterioles.

The importance of PKN2 in cardiac development and disease led us to investigate what the consequences might be with aging, comparing echocardiography data for male mice with an average age of 12 weeks with those obtained from mice with an average age of 42 weeks. As expected, hearts from the older mice had a significantly greater LV mass than the 12 week animals, but there was no difference between WT and *Pkn2*Het mice (Figure 6a). The largest diameter of the aortae (measured during cardiac systole) increased with age to some extent in both genotypes, but the distensibility of the aorta was compromised in the older mice as shown by a reduction in the ratio between the diameter measured at cardiac systole and after the aortic valve has closed when the diameter is at its narrowest (Figure 6b). This appeared to be mitigated to some degree in the *Pkn2*Het mice. Pulsed-wave Doppler was used to assess blood flow from the heart into the aorta and the pulmonary artery. We detected no differences in blood flow in either vessel in the young mice (Figure 6c–f; Supplementary Table S1). Older WT and *Pkn2*Het mice had reduced pulmonary velocity time interval (VTI), with a reduction in velocity and gradient, and the degree of change was similar (Figure 6c,d; Supplementary Table S1). In WT mice, the aortic velocity time interval (VTI), along with the mean/peak velocity and gradient were all significantly reduced in older mice compared with the young mice, but aortic VTI, velocity and gradients were relatively preserved in the older *Pkn2*Het mice (Figure 6e,f; Supplementary Table S1). This may be a consequence of greater flexibility/elasticity of the aorta in these mice compared with the WT animals (Figure 6b). This raises the possibility that some of the long survival of a minor subset of *SM22aCre^{+/-} Pkn2^{fl/fl}* mice may have been supported by loss of PKN2 in the aorta.

Overall, our studies of PKN2 in the adult heart indicate that it plays a significant role in cardiovascular adaptation to pathophysiological stresses, both in disease and as animals age, affecting both the contractile cardiomyocytes themselves and the major vessels.

Discussion

This study addresses the role of PKN2 throughout development, from its importance in cardiomyocytes in the embryo, through influence on cardiac remodelling in pathological cardiac hypertrophy in the adult heart and to a potential role in aging. It shows that there can be a continuous spectrum between heart disease defined as being ‘congenital’ and what might be considered as ‘acquired’ heart disease in adults. As previously reported [16, 17], PKN2 is critical for embryonic cardiac development but our data demonstrate that PKN2 plays a crucial role in cardiomyocytes, having a particular effect on development of the compact myocardium. PKN2 also supports cardiac remodelling in response to hypertension, but has apparently little impact on the aging heart, potentially having a greater effect on the vasculature.

Previous studies using the *SM22α* promoter in mice suggested that PKN2 is required in cardiomyocytes for embryonic cardiac development [17]. Our data, using the *XMLC* promoter for specific cardiomyocyte deletion of *Pkn2* reinforce this conclusion and *XMLC*-driven knockout of *Pkn2* was of even greater severity, with only one homozygote survivor from the *XMLC*-driven knockout. In both models, embryos were produced at a normal Mendelian ratio, but the ventricular walls of the hearts in E14.5–E18.5 embryos were very thin, and the integrity and contiguity of these walls was compromised, impacting on the overall architecture of the heart as it developed *in utero*. The heart is the earliest functioning organ to form in the embryo and, in mice, cardiac looping is generally completed by E9.0 with chamber development apparent by E9.5 [30–32]. Although looping may be delayed, cardiac development appears relatively normal through to E11.5 with *SM22α*-driven *Pkn2* knockout, with no evidence of any significant effect on cardiomyocyte proliferation or global cardiac structure [17]. Here, we showed that by E14.5, there were significant effects of *Pkn2* deletion in cardiomyocytes (Figures 1 and 3): cardiac trabeculae had developed between E9.5 and E14.5, projecting into the ventricular chambers as expected, but there was a failure in formation of the compact myocardium, resulting in thin walls. Consistent with this, amongst other changes, there is a decrease in expression of the compact layer marker, *Hey2* [33] in these mutant embryos (unpublished observations). This phase of cardiac development is still poorly understood, but cardiomyocytes required for compaction develop largely from a different pool of cells from the base of the trabeculae that are less differentiated and have higher proliferative potential [30, 31]. The compaction process requires proliferation of these cells and, although the trabecular cells contribute to the compact myocardium, they also form part of the vasculature within the myocardium and the Purkinje fibre network. PKN2 can control migration and influence intercellular adhesion in other cells (e.g. fibroblasts, epithelial cells, skeletal muscle myoblasts [14, 17, 34, 35]), factors that potentially influence cardiac compaction in embryonic development.

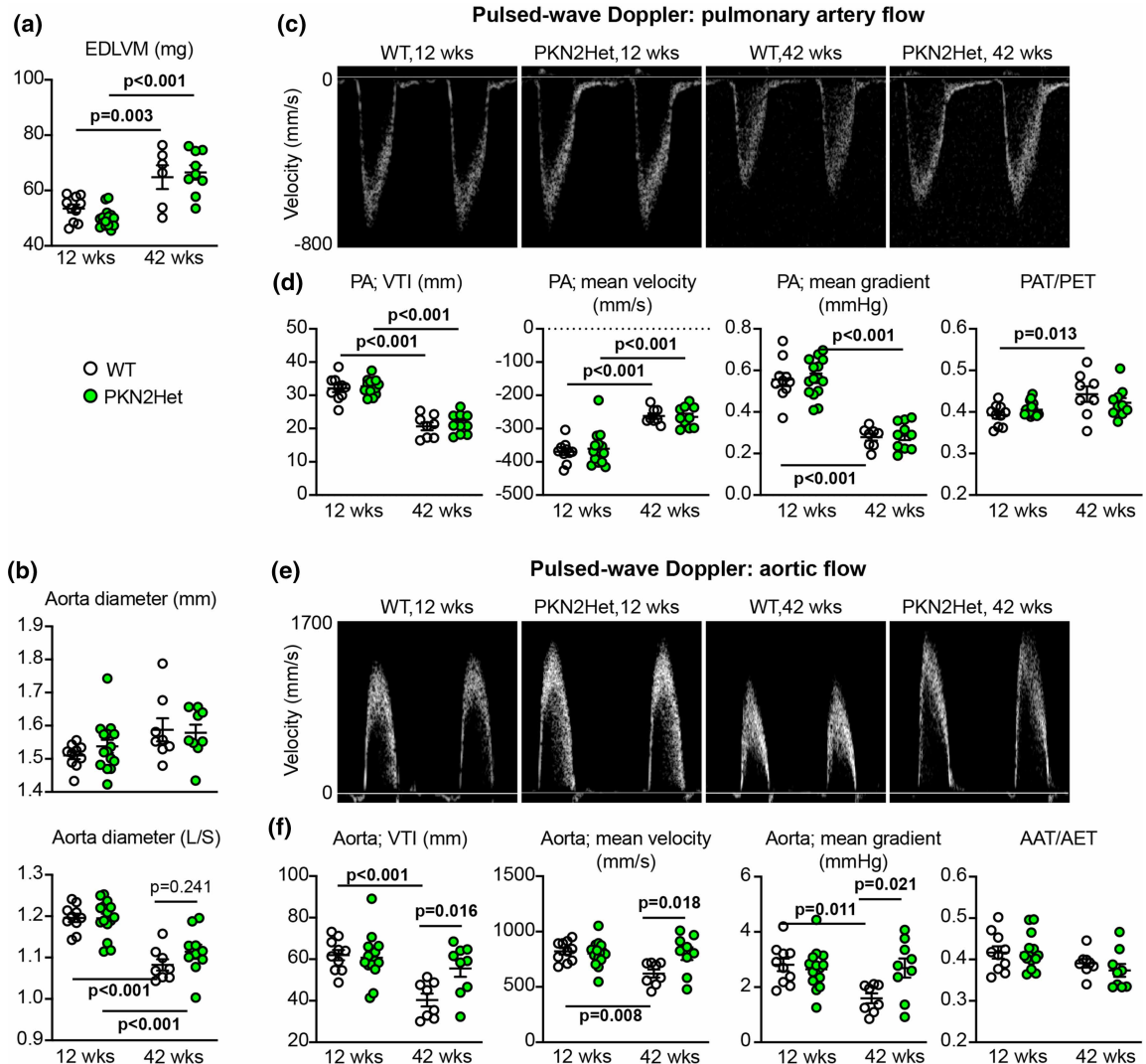


Figure 6. Effects of aging on aortic and pulmonary blood flow in WT and *Pkn2*Het mice.

Echocardiograms were taken for *Pkn2*Het and WT littermates with an average age of 12 or 42 weeks. (a), End diastolic left ventricular mass (EDLVM) was measured from long-axis B-mode images using speckle-tracking strain analysis. (b), The width of the aorta was measured from B-mode images from the widest diameter taken at cardiac systole (upper panel) and assessing the ratio of this to the narrowest diameter taken after the aortic valve closed (L/S). (c–f), Pulsed wave Döppler was used to assess blood flow as it leaves the heart into the pulmonary artery (c and d) and the aorta (e and f). Additional data are provided in Supplementary Table S1. Representative images are shown (c and e) and with the analysis (d and f). Individual data points are shown with means \pm SEM. Analysis used two-way ANOVA with Holm–Sidak’s post-test.

Although mice with cardiomyocyte *Pkn2* knockout had normal Mendelian ratios throughout embryonic development, even with the milder *SM22 α* -driven knockout model, only \sim 30% survived the perinatal phase. This is probably because of myocardial developmental malformations, in particular the lack of an adequate compact myocardium, compromising neonatal cardiac adaptation to an increased workload and oxidative metabolism, along with cell cycle withdrawal of cardiomyocyte and a switch from hyperplasia to maturational (hypertrophic) growth [32]. The data have clear implications for congenital heart disease both with respect to *PKN2* itself and its downstream signalling, particularly in relation to a potential role in the formation of the compact myocardium and left ventricular non-compaction. Although left ventricular hypertrabeculation or non-compaction is a recognised genetic disease, it varies in presentation and severity. Cardiomyocyte *Pkn2*

knockout appears to have the greatest similarity with the most severe form associated with fetal/neonatal disease that is often lethal by or within the first year of life and which (as for the *Pkn2* knockout mice) is often associated with structural cardiac abnormalities [36, 37].

Mice with heterozygous PKN2 deletion have no obvious abnormalities and cardiac development appears normal [17]. Moreover, we did not detect any profound differences in cardiac function/dimensions between WT and *Pkn2*Het mice into middle/old age (42 weeks). This means that PKN2 is largely dispensable once the heart has formed and is only required for cardiac remodelling in response to a severe stress such as that induced by sudden imposition of pressure-overload in the AngII experiments. We did detect a difference in aortic flow and the reduction in flow in the WT mice was largely prevented in the *Pkn2*Het mice. The meaning of this is not currently clear, but there may be some adaptation of the aorta that preserved LV function. The difference was not apparent in pulmonary flow suggesting that the effect was specific for the highly muscularised aortic wall.

Even though it may have little role in a non-stressed heart, PKN2 is important in the adult cardiac response to pathophysiological stressors since expression is increased in patients with DCM and in mouse hearts subjected to pressure-overload resulting from AngII treatment. In our hands, PKN2 haploinsufficiency compromised cardiac adaptation to AngII, with reduced LV hypertrophy and an overall reduction in the increase in the LV mass, resulting from inhibition of cardiomyocyte enlargement and fibrotic ECM. This contrasts with a recent study reporting that tamoxifen-inducible, cardiomyocyte-specific knockout of both PKN1 or PKN2 (not either gene alone) in adult mice, reduced cardiac hypertrophy in models of pressure-overload, namely thoracic aortic constriction (TAC) or AngII [25]. The most obvious difference is our use of global heterozygotes rather than cardiomyocyte-specific knockout, and inhibition of fibrosis induced by AngII in our studies may result from PKN2 haploinsufficiency in cardiac non-myocytes, causing a reduction in fibrosis that reduces cardiomyocyte workload. Alternatively, the effect may be due to PKN2 haploinsufficiency in cardiomyocytes, and the differences reflect the higher degree of stress imposed on the heart in our studies (0.8 mg/kg/d AngII) compared with Sakaguchi et al., who used 0.1 mg/kg/d, a sub- or slow pressor dose [38]. Another difference is the duration of the experiment, here the study was conducted over 7 d, whilst the study by Sakaguchi et al. was over 28 d. It is possible that the heart may adapt such that differences in function/dimensions are no longer apparent by 28 d, however, our experience is that the phenotype becomes more pronounced with prolonged duration of treatment as heart failure develops [29]. With global knockout, there are also potential systemic effects on the heart that influence cardiac adaptation to AngII. Although PKN2 does not appear to play a significant role in endothelial cells during development [17], endothelial cell specific knockout in adult mice increases blood pressure *in vivo*, potentially due to loss of phosphorylation of eNOS with consequent reduction in NO production in the peripheral vasculature. There was no evidence for this in our studies of mice with global PKN2 haploinsufficiency, with no increase in fibrosis or cardiomyocyte hypertrophy at baseline. Furthermore, we detected no difference in phosphorylation of eNOS (data not shown). A final consideration relating to all of these studies is the background strain of the mice. Our studies used mice with a C57Bl/6J background, rather than C57Bl/6N and the cardiac responses of these two strains can differ substantially (see, for example, [39]).

The PKN family of enzymes remain poorly understood. PKN1 is the most well-investigated and is implicated in protection against ischaemia/reperfusion injury in *ex vivo* models but, even for this family member, there is little information on mechanism of action. For PKN2, there is less. It may influence gene expression directly via interaction and phosphorylation of HDAC5 [40], preventing HDAC5 import into the nucleus and thus increasing chromatin remodelling or it may act via MRTF to regulate hypertrophy-associated gene expression [25]. Our RNASeq data are not consistent with this because, although AngII induced changes in gene expression as expected with increases in classic hypertrophy-associated gene expression (e.g. *Nppa*, *Myh7*, *Nppb*), there was no apparent effect of *Pkn2* haploinsufficiency. Instead, *Pkn2* haploinsufficiency had a more general effect to moderate the changes induced by AngII on collagen production, mitochondrial TCA genes, interferon response genes and genes in the complement system (it is noted that mitochondrial TCA gene expression is also down-regulated in embryonic hearts from *SM22 α -Cre^{+/-} Pkn2^{fl/fl}* mice; data not shown). The net effect would be to maintain cardiac energetics, reduce inflammation and reduce fibrosis. The marked inhibition of the induction of Transgelin (*Tagln*, or *SM22 α*) upon AngII treatment of *Pkn2*Het mice compared with WT littermates, suggests a potential mechanism. *SM22 α* is an actin binding protein although its function is still obscure. In vascular smooth muscle cells, *SM22 α* facilitates stress fibre formation and contractility [41] so, with reduced *SM22 α* , the response to AngII would be dampened in *Pkn2*Het mice, as observed. The mechanism for *SM22 α* up-regulation may be due to hypoxia and activation of HIF2 α [42].

Irrespective of the mechanism of action, this study adds to an increasing body of work indicating that the PKNs play an important role in cardiac remodelling in the adult; for PKN2, haploinsufficiency impacting the response to AngII and on early knockout (driven by *XMLC2* or *SM22 α*) formation of the heart during development. With further understanding of regulation, specific targets and functions, PKN signalling may offer therapeutic options for managing congenital and adult heart diseases. This undoubtedly requires further research but, since the PKNs are not redundant and have specific roles in different cells/tissues, it will be essential to develop specific tools for inhibition and manipulation of the different family members.

The ROCK inhibitor Fasudil is a known broad specificity PKN inhibitor [43], already in clinical use in Japan and China as a vasodilator [44]. More discriminating inhibitors are necessary and, although it may prove challenging to target individual PKNs by small molecule approaches [43], other approaches may be useful. For example, an siRNA against *PKN3* (*Atu027*) has been in clinical trials as a novel chemotherapeutic agent for solid cancers and pancreatic cancer (in combination with Gemcitabine) [45–47], and exogenous application of the auto-inhibitory PLK peptide from PKN1 has been explored also [48]. Similar approaches might work for PKN2 [49] and, as with other protein kinases, developing these inhibitory systems will not only form the basis for novel therapeutics for the future, but their use as biochemical tools to elucidate mechanisms of action can facilitate the identification of other targets in the pathway.

Materials and methods

Mouse strains, *in vivo* mouse imaging and experiments, and *ex vivo* imaging

*Pkn2*Het, floxed *Pkn2* and *SM22 α -Cre* mouse strains were maintained on a C57Black6J background, and each sourced as described in Quetier et al. [17]. The *XMLC2-Cre* mouse strain [26] was provided from within the Francis Crick Institute and was on a mixed background, subsequently in this study back-crossed onto the C57Black6J background. Most Cre mice in this study also carried the mTmG reporter allele at the *Rosa26* locus, sourced as described previously [17]. Genotyping was carried out by Transnetyx using real-time PCR, with methods based upon the PCR genotyping described in Quetier et al. [17].

In vivo imaging of mice from *SM22 α -Cre* and *XMLC2-Cre* crosses was carried out at UCL-CABI (up to 2017; *SM22 α -Cre* only) or the Francis Crick Institute (post 2017). MRI, micro-CT and ultrasound imaging technologies were utilised. All *in vivo* mouse imaging was carried out under continuous inhalation anaesthesia using isoflurane (1.5–5%) supplied with oxygen at 1–2 L/min, and with appropriate restraint. We note 5% isoflurane was used to induce anaesthesia initially, and maintenance was typically at 1.5–2%, but some strongly phenotypic *SM22 α -Cre^{+/-}-Pkn2^{fl/fl}* mice required higher levels of isoflurane for successful maintenance. Procedures typically lasted only 20 min, with exception for cine-MRI, which necessitated longer non-recovery procedures. At UCL-CABI, the micro-CT was performed on mice in the supine position in a nanoScanPET/CT scanner (Mediso, Hungary) with a 50 kVp X-ray source, with 300 ms exposure time in 720 projections with an acquisition time of 8 min. Ultrasound of young *PKN2*Het mice (at St. George's University of London) and of a subset of *SM22 α -Cre^{+/-}-Pkn2^{fl/fl}* mice (at UCL-CABI) was performed using VEVO2100 ultrasound machines (VisualSonics Inc., Toronto, ON, Canada) with MS400 18–38 MHz transducer mouse probes, whilst middle-aged mice were imaged using a VEVO3100 with a MS-550D 25–55 MHz transducer. Mice were restrained on a heated VEVO Imaging Station, and cardiac scans of the parasternal long-axis and short-axis were recorded in B mode and M mode, and flow velocity waveforms of the aorta near the aortic valve were obtained with colour Doppler and then placing the pulsed wave Doppler sample gate over the colour Doppler signals. The ultrasound used at the Francis Crick Institute was a VEVO3100, but otherwise scans were performed as described above. At the Francis Crick Institute, cardiac cine-MRI was performed using a 9.4T MRI (Bruker GmbH) equipped with a four-channel receive only mouse cardiac coil and 86 mm volume transmit coil, and Paravision 6.0.1 software. Mice were set up lying prone head-first with a heat pad and breathing movement sensor pad. A series of fast low-angle shot (FLASH) scans used for localisation of the heart and to determine the short-axis. Short-axis retrospectively-gated cine-MRI (intra-gate-FLASH sequence) was performed using the following parameters: 0.8 mm slices covering the entire left and right ventricles; 128 × 128 pixels matrix and field of view of 25 × 25 mm, giving a resolution of ~195 μ m; TR = 5.5 ms, TE = 2.233 ms, 10° flip angle; 300× oversampling with 24 cine frames reconstruction.

MRI data was converted using in-house MATLAB scripts to obtain tiffs, followed by ImageJ for image analysis, following published procedures [50]. This entailed determining the area of lumen in each the LV and RV in each slice at each systole and diastole, and calculating an approximate volume for the lumens of LV and RV at each systole and diastole based on the slice thickness of 0.8 mm. Stroke volumes and the ejection fractions

were determined by comparing diastolic and systolic chamber volumes. The relative volumes of the LV and RV, and number of slices containing LV and RV enabled assessment of abnormalities of shape of the hearts, as reported in Results.

Ex vivo imaging of 10% buffered formalin-fixed, and subsequently PBS-soaked (24 h) whole carcasses or extracted plucks (heart and lungs) from a cohort of mice from the SM22 α -Cre crosses was carried out at the Francis Crick Institute by micro-CT using a SkyScan1176 CT scanner (Bruker MicroCT, Kontich, Belgium). Three-hundred and ninety-four projections were acquired over a 180° trajectory with an exposure time of 65 ms, frame averaging of 3, X-ray source voltage and current of 50 kV and 500 μ A, and a 0.5 mm Al filter. Scans were reconstructed at a 34.2 μ m isotropic resolution using nRecon software (version 1.6.10.1, Bruker MicroCT). Video 2 was generated by segmentation of heart, lungs and cardiac calcification using Analyze (version 12.0, AnalyzeDirect, Overland Park, KS, U.S.A.) using threshold based segmentation.

For *in vivo* basal and AngII-challenge studies with young mice, male *Pkn2*Het and wild-type (WT) littermates (average age 11 weeks) on a C57Bl/6J background were imported into the BioResource Facility at St. George's University of London and allowed to acclimatise for 7 d. Mice were randomly allocated to each treatment group; body weights are provided in Supplementary Table S10. Drug delivery used 1007D Alzet osmotic pumps, filled according to the manufacturer's instructions. Mice received minipumps for delivery of 0.8 mg/kg/d AngII (Merck) or vehicle (acidified PBS). Minipumps were incubated overnight in sterile PBS (37°C), then implanted subcutaneously under continuous inhalation anaesthesia using isoflurane (induction at 5%, maintenance at 2–2.5%) mixed with 2 l/min O₂. A 1 cm incision was made in the mid-scapular region and mice were given 0.05 mg/kg (s.c.) buprenorphine (Ceva Animal Health Ltd.) to repress post-surgical discomfort. Minipumps were implanted portal first in a pocket created in the left flank region of the mouse. Wound closure used a simple interrupted suture with polypropylene 4-0 thread (Prolene, Ethicon). Mice were allowed to recover singly and returned to their home cage once fully recovered. Echocardiography was performed on anaesthetised mice using the VEVO2100 imaging system equipped with a MS400 18–38 MHz transducer (Visualsonics). Mice were anaesthetised in an induction chamber with isoflurane (5% flow rate) with 1 l/min O₂ then transferred to the heated Vevo Imaging Station. Anaesthesia was maintained with 1.5% isoflurane delivered via a nose cone. Baseline scans were taken prior to experimentation (–7 to –3 days). Further scans were taken at intervals following tamoxifen treatment or minipump implantation. Imaging was completed within 20 min. Mice were recovered singly and transferred to the home cage once fully recovered.

For *in vivo* studies with middle-aged mice, male *Pkn2*Het and wild-type (WT) littermates (average age 42 weeks) were housed in the Francis Crick Institute and echocardiograms were taken with the VEVO3100 imaging system (Visualsonics).

Data analysis was performed using VevoLAB software (Visualsonics) by an independent assessor blinded to any AngII intervention. Left ventricular cardiac dimensions were assessed from short axis M-mode images with the axis placed at the mid-level of the left ventricle at the level of the papillary muscles. Data were gathered from two M-mode scans at each time point, taking mean values across four cardiac cycles for each echocardiogram. The diameter of the aorta was measured with the calliper function from B-mode images at the end of cardiac systole (with the aorta at its widest) and following aortic contraction, taking an average of measurements across two cardiac cycles. Cardiac function and left ventricular mass were measured B-mode long axis images using Vevo Strain software for speckle tracking. Blood flow was assessed using pulsed-wave Doppler.

Mice were killed either by cervical dislocation followed by exsanguination, or by CO₂ inhalation followed by cervical dislocation. Hearts were excised quickly, washed in PBS and blotted to remove excess PBS. The apex of the heart was snap-frozen in liquid N₂ and the remainder fixed in 10% buffered formalin for histology.

Ethics statement for adult mouse experiments

Animals were housed in the Biological Resource Unit (BRU) at Cancer Research UK's London Research Institute (LRI to 2016), University College London (UCL)'s Centre for Advanced Biomedical Imaging (for pilot imaging experiments) and the Biological Research Facility (BRF) at the Francis Crick Institute (from 2016 onward), or the BioResource Facility at St. George's University of London. Each site is UK registered with a Home Office certificate of designation. Studies were performed in accordance with European Parliament Directive 2010/63/EU on the protection of animals used for scientific purposes, institutional animal care committee procedures (CRUK's London Research Institute, University College London, The Francis Crick Institute, University of Reading and St. George's University of London) and the UK Animals (Scientific Procedures) Act

1986 (under Procedure Project Licences 77/8066, P166DEA98, 70/7474, 70/8248, 70/8249, 70/8709 and P8BAB0744).

HREM, histology and assessment of myocyte size and fibrosis

Samples for high resolution episcopic microscopy (HREM) were fixed in Bouin's for a minimum of 12 h followed by extensive washing in PBS, dehydration in a graded methanol series, incubation in JB-4 (Sigma)/Eosine (Sigma)/Acridine orange (Sigma) mix overnight to ensure proper sample infiltration and then embedded in fresh mix by adding the accelerator (see [51]). Once polymerised the blocks were imaged as previously described [52, 53]; details of the process can be found at: <https://dmdd.org.uk/hrem/>. Samples were sectioned on a Leica sledge microtome at 1 or 2 μm or on a commercial HREM (Indigo Scientific) at 0.85 or 1.7 μm . An image of the surface of the block was then acquired under GFP excitation wavelength light using Olympus MVX10 microscope and a high resolution camera (Jenoptik). After acquisition the stacks were adjusted for gray levels using Photoshop CS6 and then processed for isotropic scaling, orthogonal resectioning, 25% down-scaling, using a mixture of commercial and homemade software (see Wilson R et al. NAR 2016, Vol. 44 D855–D861). 3D volume renderings of the datasets were typically produced from the 25% downscaled stack using OsirixMD or Horos.

Histological staining and analysis were performed as previously described [28], by board certified veterinary pathologists, assessing general morphology by haematoxylin and eosin (H&E), general fibrosis by Masson's or Gomori's trichrome (as indicated in figure legends and below) and collagen deposition using picrosirius red (PSR). Images of heart sections were captured and stored digitally using a Hamamatsu slide scanner. For analysis of myocyte cross-sectional area, cells stained by H&E within the LV (excluding epicardial and endocardial regions) were outline traced using NDP.view2 software (Hamamatsu). Only cells with a single nucleus that were clearly in cross-section were included in the analysis, and all cells in a given area meeting these criteria were measured. For assessment of interstitial fibrosis, PSR-stained sections were used and the areas of the myocardium in the middle of the left ventricular free wall, plus the points of intersection between the left ventricle and the interventricular septum were scored (0, no fibrosis; 1, limited fibrosis; 2, significant fibrosis; 3, extensive fibrosis permeating the tissue) and the mean value taken for each mouse. To assess perivascular fibrosis, Masson's Trichrome images were used. All arteries/arterioles with a clearly defined elastic lamina in cross section were measured across the diameter. Vessels $>20 \mu\text{m}$ diameter were scored as for interstitial fibrosis. The mean values for each mouse were taken. Data analysis was performed by an independent assessor blinded to treatment groups.

RNASeq, qPCR and immunoblotting of adult mouse heart samples

The apex of each of the mouse hearts was ground to powder under liquid N_2 . Samples (10–15 mg) were homogenised with 1 ml RNA Bee (AMS Biotechnology Ltd). RNA was prepared according to the manufacturer's instructions and dissolved in nuclease-free water. The concentration and purity were assessed from the A_{260} and A_{260}/A_{280} values measured using an Implen NanoPhotometer.

The nf-core/rnaseq pipeline version 3.1 [54] was used to prepare quantified expression matrices. The pipeline takes FastQ files as input and runs quality control checks on the data, trims reads for low quality nucleotides, aligns reads and quantifies aligned data to gene models. The GRCm38 reference and Ensembl release-95 gene models were provided. The '-aligner star_rsem' option was specified to align the reads with STAR [55] and quantify expression with RSEM [56] via RSEM version 1.3.1. Raw gene-level counts were imported into R using tximport [57] and DESeq2 version 1.32.0 [58] used to test for differential expression with a FDR threshold of 1%.

Quantitative PCR (qPCR) was performed as previously described [59]. Total RNA (0.5 μg) was reverse transcribed to cDNA using High Capacity cDNA Reverse Transcription Kits with random primers (Applied Biosystems) according to the manufacturer's instructions. qPCR was performed using an ABI Real-Time PCR 7500 system (Applied Biosystems) using optical 96-well reaction plates and iTaq Universal SYBR Green Supermix (Bio-Rad Laboratories Inc.). *GAPDH* was used as the reference gene for the study. Results were normalised to *GAPDH*, and relative quantification was obtained using the ΔCt (threshold cycle) method; relative expression was calculated as $2^{-\Delta\Delta\text{Ct}}$, and normalised to vehicle or time 0. Primers were from Eurofins Genomics; sequences are provided in Supplementary Table S11.

Samples of heart powders (10–15 mg) were extracted in 8 vol (relative to powder weight) Buffer A [20 mM Tris pH 7.5, 1 mM EDTA, 10% (v/v) glycerol, 1% (v/v) Triton X-100, 100 mM KCl, 5 mM NaF, 0.2 mM

Na₃VO₄, 5 mM MgCl₂, 0.05% (v/v) 2-mercaptoethanol, 10 mM benzamidine, 0.2 mM leupeptin, 0.01 mM trans-epoxy succinyl-l-leucylamido-(4-guanidino)butane, 0.3 mM phenylmethylsulphonyl fluoride, 4 μM microcystin]. Samples were vortexed and extracted on ice (10 min). Extracts were centrifuged (10 000×g, 10 min, 4°C). The supernatants were removed, a sample was taken for protein assay and the remainder boiled with 0.33 vol sample buffer [0.33 M Tris-HCl pH 6.8, 10% (w/v) SDS, 13% (v/v) glycerol, 133 M dithiothreitol, 0.2 mg/ml bromophenol blue]. Protein concentrations were determined by Bio-Rad Bradford assay using bovine serum albumin (BSA) standards.

Proteins were separated by SDS-PAGE using using a Bio-Rad mini-gel system with 8% (w/v) polyacrylamide resolving gels and 6% stacking gels (200 V, 90 min) for PKN1/2 (40 μg total protein), or 12% polyacrylamide resolving gels and 6% stacking gels (200 V, 50 min) for GAPDH (5 μg total protein). Proteins were transferred electrophoretically to nitrocellulose using a Bio-Rad semi-dry transfer cell (10 V, 60 min) and detected as previously described [59]. Bands were visualised by enhanced chemiluminescence using ECL Prime Western Blotting detection reagents and using an ImageQuant LAS4000 system (GE Healthcare). ImageQuant TL 8.1 software (GE Healthcare) was used for densitometric analysis. Raw values for phosphorylated PKN1/2 were normalised to the total kinase. Values for all samples were normalised to the mean of the controls. Primary antibodies for total PKN2 (Cat. No. 2612), phospho-PKN1/2 (Cat. No. 2611) and GAPDH (Cat. No. 2118) were from Cell Signalling Technology. Antibodies for PKN1 were from BD Transduction Laboratories (Cat. No. 610686). Phospho- and total PKN antibodies were used at 1/750 dilution; GAPDH antibodies were used at 1/1000 dilution.

Bioinformatics analysis for transcript expression in dilated cardiomyopathy

mRNA expression of *PKN1* (ENSG00000123143), *PKN2* (ENSG00000065243) and *PKN3* (ENSG00000160447) in control and diseased human hearts was determined using a published RNASeq dataset for left ventricular samples of 97 patients with end-stage dilated cardiomyopathy taken at the time of transplantation or left ventricular assist device implantation, and 108 non-diseased controls [27]. Differential expression analysis was carried out using DESeq2 (V1.18.1, Wald test) [58].

Data Availability

The RNA sequence data generated in this study is available through GEO at GSE206779.

Competing Interests

The authors declare that there are no competing interests associated with the manuscript.

Funding

J.J.T.M., T.S., B.S., A.S.-B., E.H., S.L.P., T.M. and P.J.P. were supported by the Francis Crick Institute which receives its core funding from Cancer Research UK (CRUK) (FC001130), the UK Medical Research Council (MRC) (FC001130), and the Wellcome Trust (FC001130). A.C. acknowledges support from the British Heart Foundation FS/18/33/33621 (J.J.C.) and Qassim University, Saudi Arabia (H.O.A.). D.J.S. was supported by British Heart Foundation Intermediate and Senior Basic Science Research Fellowships (FS/15/33/31608, FS/SBSRF/21/31020), the BHF Centre for Regenerative Medicine RM/17/1/33377, the MRC MR/R026416/1, and the Wellcome Trust 212937/Z/18/Z. S.T.E.C. and D.M. were supported by BHF studentship FS/19/24/34262 and the Wellcome Trust 204809/16/z.

CRedit Author Contribution

Peter J. Parker: Conceptualization, Resources, Formal analysis, Supervision, Funding acquisition, Writing — original draft, Project administration, Writing — review and editing. **Jacqueline JT Marshall:** Conceptualization, Formal analysis, Investigation, Writing — original draft, Project administration, Writing — review and editing.

Joshua J. Cull: Investigation, Writing — review and editing. **Hajed O. Alharbi:** Investigation, Writing — review and editing. **May Zaw Thin:** Investigation, Writing — review and editing. **Susanna TE Cooper:** Investigation, Writing — review and editing. **Christopher Barrington:** Formal analysis, Writing — review and editing.

Hannah Vanyai: Investigation, Writing — review and editing. **Thomas Snoeks:** Investigation, Writing — review and editing. **Bernard Siow:** Investigation, Writing — review and editing. **Alejandro Suarez-Bonnet:** Investigation, Writing — review and editing. **Eleanor Herbert:** Investigation, Writing — review and editing.

Daniel J. Stuckey: Investigation, Writing — review and editing. **Angus Cameron:** Conceptualization, Supervision,

Investigation, Writing — review and editing. **Fabrice Prin:** Investigation, Writing — review and editing. **Andrew C. Cook:** Conceptualization, Writing — review and editing. **Simon L. Priestnall:** Investigation, Writing — review and editing. **Sonia Chotani:** Investigation, Writing — review and editing. **Owen JL Rackham:** Investigation, Writing — review and editing. **Daniel Meijles:** Conceptualization, Supervision, Investigation, Writing — review and editing. **Timothy Mohun:** Supervision, Investigation, Writing — review and editing. **Angela Clerk:** Conceptualization, Resources, Supervision, Investigation, Writing — original draft, Writing — review and editing.

Abbreviations

AngII, angiotensin II; DCM, dilated cardiomyopathy; DEGs, differentially expressed genes; FDR, false discovery rates; HREM, high resolution episcopic microscopy; LV, left ventricle; PKN, protein kinase N; PSR, picosirius red; TAC, transverse aortic constriction; TCA, tricarboxylic acid; VTI, velocity time interval.

References

- Bouma, B.J. and Mulder, B.J. (2017) Changing landscape of congenital heart disease. *Circ. Res.* **120**, 908–922 <https://doi.org/10.1161/CIRCRESAHA.116.309302>
- Hoffman, J.I. and Kaplan, S. (2002) The incidence of congenital heart disease. *J. Am. Coll. Cardiol.* **39**, 1890–1900 [https://doi.org/10.1016/S0735-1097\(02\)01886-7](https://doi.org/10.1016/S0735-1097(02)01886-7)
- Jankauskas, S.S., Kansakar, U., Varzideh, F., Wilson, S., Mone, P., Lombardi, A. et al. (2021) Heart failure in diabetes. *Metabolism* **125**, 154910 <https://doi.org/10.1016/j.metabol.2021.154910>
- Messerli, F.H., Rimoldi, S.F. and Bangalore, S. (2017) The transition from hypertension to heart failure: contemporary update. *JACC Heart Fail.* **5**, 543–551 <https://doi.org/10.1016/j.jchf.2017.04.012>
- Ponikowski, P., Anker, S.D., AlHabib, K.F., Cowie, M.R., Force, T.L., Hu, S. et al. (2014) Heart failure: preventing disease and death worldwide. *ESC Heart Fail.* **1**, 4–25 <https://doi.org/10.1002/ehf2.12005>
- Savarese, G. and Lund, L.H. (2017) Global public health burden of heart failure. *Card. Fail. Rev.* **3**, 7–11 <https://doi.org/10.15420/cfr.2016.25.2>
- Walli-Attaei, M., Joseph, P., Rosengren, A., Chow, C.K., Rangarajan, S., Lear, S.A. et al. (2020) Variations between women and men in risk factors, treatments, cardiovascular disease incidence, and death in 27 high-income, middle-income, and low-income countries (PURE): a prospective cohort study. *Lancet* **396**, 97–109 [https://doi.org/10.1016/S0140-6736\(20\)30543-2](https://doi.org/10.1016/S0140-6736(20)30543-2)
- Wenzl, F.A., Ambrosini, S., Mohammed, S.A., Kraler, S., Luscher, T.F., Costantino, S. et al. (2021) Inflammation in metabolic cardiomyopathy. *Front. Cardiovasc. Med.* **8**, 742178 <https://doi.org/10.3389/fcvm.2021.742178>
- Ahuja, P., Sdek, P. and MacLellan, W.R. (2007) Cardiac myocyte cell cycle control in development, disease, and regeneration. *Physiol. Rev.* **87**, 521–544 <https://doi.org/10.1152/physrev.00032.2006>
- Broughton, K.M. and Sussman, M.A. (2019) Adult cardiomyocyte cell cycle detour: Off-ramp to quiescent destinations. *Trends Endocrinol. Metab.* **30**, 557–567 <https://doi.org/10.1016/j.tem.2019.05.006>
- Dorn, II, G.W., Robbins, J. and Sugden, P.H. (2003) Phenotyping hypertrophy: eschew obfuscation. *Circ. Res.* **92**, 1171–1175 <https://doi.org/10.1161/01.RES.0000077012.11088.BC>
- Fuller, S.J., Osborne, S.A., Leonard, S.J., Hardyman, M.A., Vaniotis, G., Allen, B.G. et al. (2015) Cardiac protein kinases: the cardiomyocyte kinase and differential kinase expression in human failing hearts. *Cardiovasc. Res.* **108**, 87–98 <https://doi.org/10.1093/cvr/cvz210>
- Marrocco, V., Bogomolovas, J., Ehler, E., Dos Remedios, C.G., Yu, J., Gao, C. et al. (2019) PKC and PKN in heart disease. *J. Mol. Cell. Cardiol.* **128**, 212–226 <https://doi.org/10.1016/j.yjmcc.2019.01.029>
- Lachmann, S., Jevons, A., De Rycker, M., Casamassima, A., Radtke, S., Collazos, A. et al. (2011) Regulatory domain selectivity in the cell-type specific PKN-dependence of cell migration. *PLoS ONE* **6**, e21732 <https://doi.org/10.1371/journal.pone.0021732>
- Palmer, R.H., Ridder, J. and Parker, P.J. (1995) Cloning and expression patterns of two members of a novel protein-kinase-C-related kinase family. *Eur. J. Biochem.* **227**, 344–351 <https://doi.org/10.1111/j.1432-1033.1995.tb20395.x>
- Danno, S., Kubouchi, K., Mehruha, M., Abe, M., Natsume, R., Sakimura, K. et al. (2017) PKN2 is essential for mouse embryonic development and proliferation of mouse fibroblasts. *Genes Cells* **22**, 220–236 <https://doi.org/10.1111/gtc.12470>
- Quetier, I., Marshall, J.J.T., Spencer-Dene, B., Lachmann, S., Casamassima, A., Franco, C. et al. (2016) Knockout of the PKN family of Rho effector kinases reveals a Non-redundant role for PKN2 in developmental mesoderm expansion. *Cell Rep.* **14**, 440–448 <https://doi.org/10.1016/j.celrep.2015.12.049>
- Lepore, J.J., Cheng, L., Min Lu, M., Mericko, P.A., Morrisey, E.E. and Parmacek, M.S. (2005) High-efficiency somatic mutagenesis in smooth muscle cells and cardiac myocytes in SM22alpha-Cre transgenic mice. *Genesis* **41**, 179–184 <https://doi.org/10.1002/gene.20112>
- Li, L., Miano, J.M., Cserjesi, P. and Olson, E.N. (1996) SM22 alpha, a marker of adult smooth muscle, is expressed in multiple myogenic lineages during embryogenesis. *Circ. Res.* **78**, 188–195 <https://doi.org/10.1161/01.RES.78.2.188>
- Malhowski, A.J., Hira, H., Bashiruddin, S., Warburton, R., Goto, J., Robert, B. et al. (2011) Smooth muscle protein-22-mediated deletion of Tsc1 results in cardiac hypertrophy that is mTORC1-mediated and reversed by rapamycin. *Hum. Mol. Genet.* **20**, 1290–1305 <https://doi.org/10.1093/hmg/ddq570>
- Miano, J.M., Ramanan, N., Georger, M.A., de Mesy Bentley, K.L., Emerson, R.L., Balza, Jr, R.O. et al. (2004) Restricted inactivation of serum response factor to the cardiovascular system. *Proc. Natl Acad. Sci. U.S.A.* **101**, 17132–17137 <https://doi.org/10.1073/pnas.0406041101>
- Zhang, J.C., Kim, S., Helmke, B.P., Yu, W.W., Du, K.L., Lu, M.M. et al. (2001) Analysis of SM22alpha-deficient mice reveals unanticipated insights into smooth muscle cell differentiation and function. *Mol. Cell. Biol.* **21**, 1336–1344 <https://doi.org/10.1128/MCB.2001.21.4.1336-1344.2001>
- Takagi, H., Hsu, C.P., Kajimoto, K., Shao, D., Yang, Y., Maejima, Y. et al. (2010) Activation of PKN mediates survival of cardiac myocytes in the heart during ischemia/reperfusion. *Circ. Res.* **107**, 642–649 <https://doi.org/10.1161/CIRCRESAHA.110.217554>

- 24 Francois, A.A., Obasanjo-Blackshire, K., Clark, J.E., Boguslavskyi, A., Holt, M.R., Parker, P.J. et al. (2018) Loss of Protein Kinase Novel 1 (PKN1) is associated with mild systolic and diastolic contractile dysfunction, increased phospholamban Thr17 phosphorylation, and exacerbated ischaemia-reperfusion injury. *Cardiovasc. Res.* **114**, 138–157 <https://doi.org/10.1093/cvr/cvx206>
- 25 Sakaguchi, T., Takefuji, M., Wettshureck, N., Hamaguchi, T., Amano, M., Kato, K. et al. (2019) Protein kinase N promotes stress-induced cardiac dysfunction through phosphorylation of myocardin-Related transcription factor A and disruption of its interaction With actin. *Circulation* **140**, 1737–1752 <https://doi.org/10.1161/CIRCULATIONAHA.119.041019>
- 26 Breckenridge, R., Kotecha, S., Towers, N., Bennett, M. and Mohun, T. (2007) Pan-myocardial expression of Cre recombinase throughout mouse development. *Genesis* **45**, 135–144 <https://doi.org/10.1002/dvg.20275>
- 27 Heinig, M., Adriaens, M.E., Schafer, S., van Deutekom, H.W.M., Lodder, E.M., Ware, J.S. et al. (2017) Natural genetic variation of the cardiac transcriptome in non-diseased donors and patients with dilated cardiomyopathy. *Genome Biol.* **18**, 170 <https://doi.org/10.1186/s13059-017-1286-z>
- 28 Meijles, D.N., Cull, J.J., Markou, T., Cooper, S.T.E., Haines, Z.H.R., Fuller, S.J. et al. (2020) Redox regulation of cardiac ASK1 (Apoptosis signal-Regulating kinase 1) controls p38-MAPK (mitogen-activated protein kinase) and orchestrates cardiac remodeling to hypertension. *Hypertension* **76**, 1208–1218 <https://doi.org/10.1161/HYPERTENSIONAHA.119.14556>
- 29 Meijles, D.N., Cull, J.J., Cooper, S.T.E., Markou, T., Hardyman, M.A., Fuller, S.J. et al. (2021) The anti-cancer drug dabrafenib is not cardiotoxic and inhibits cardiac remodelling and fibrosis in a murine model of hypertension. *Clin. Sci. (Lond)* **135**, 1631–1647 <https://doi.org/10.1042/CS20210192>
- 30 Choquet, C., Kelly, R.G. and Miquerol, L. (2019) Defects in trabecular development contribute to left ventricular noncompaction. *Pediatr. Cardiol.* **40**, 1331–1338 <https://doi.org/10.1007/s00246-019-02161-9>
- 31 D'Amato, G., Luxan, G. and de la Pompa, J.L. (2016) Notch signalling in ventricular chamber development and cardiomyopathy. *FEBS J.* **283**, 4223–4237 <https://doi.org/10.1111/febs.13773>
- 32 Tan, C.M.J. and Lewandowski, A.J. (2020) The transitional heart: from early embryonic and fetal development to neonatal life. *Fetal Diagn. Ther.* **47**, 373–386 <https://doi.org/10.1159/000501906>
- 33 Koibuchi, N. and Chin, M.T. (2007) CHF1/Hey2 plays a pivotal role in left ventricular maturation through suppression of ectopic atrial gene expression. *Circ. Res.* **100**, 850–855 <https://doi.org/10.1161/01.RES.0000261693.13269.bf>
- 34 Lim, M.A., Yang, L., Zheng, Y., Wu, H., Dong, L.Q. and Liu, F. (2004) Roles of PDK-1 and PKN in regulating cell migration and cortical actin formation of PTEN-knockout cells. *Oncogene* **23**, 9348–9358 <https://doi.org/10.1038/sj.onc.1208147>
- 35 Zeng, R., Wang, Z., Li, X., Chen, Y., Yang, S. and Dong, J. (2020) Cyclin-dependent kinase 1-mediated phosphorylation of protein kinase N1 promotes anchorage-independent growth and migration. *Cell Signal.* **69**, 109546 <https://doi.org/10.1016/j.cellsig.2020.109546>
- 36 Udeoji, D.U., Philip, K.J., Morrissey, R.P., Phan, A. and Schwarz, E.R. (2013) Left ventricular noncompaction cardiomyopathy: updated review. *Ther. Adv. Cardiovasc. Dis.* **7**, 260–273 <https://doi.org/10.1177/1753944713504639>
- 37 Ursell, P.C. (2013) Noncompaction in the fetus and neonate: an autopsy study. *Am. J. Med. Genet. C Semin. Med. Genet.* **163C**, 169–177 <https://doi.org/10.1002/ajmg.c.31367>
- 38 Kawada, N., Imai, E., Karber, A., Welch, W.J. and Wilcox, C.S. (2002) A mouse model of angiotensin II slow pressor response: role of oxidative stress. *J. Am. Soc. Nephrol.* **13**, 2860–2868 <https://doi.org/10.1097/01.ASN.0000035087.11758.ED>
- 39 Zi, M., Stafford, N., Prehar, S., Baudoin, F., Oceandy, D., Wang, X. et al. (2019) Cardiac hypertrophy or failure?: a systematic evaluation of the transverse aortic constriction model in C57BL/6NTac and C57BL/6J substrains. *Curr. Res. Physiol.* **1**, 1–10 <https://doi.org/10.1016/j.crphys.2019.10.001>
- 40 Harrison, B.C., Huynh, K., Lundgaard, G.L., Helmke, S.M., Perryman, M.B. and McKinsey, T.A. (2010) Protein kinase C-related kinase targets nuclear localization signals in a subset of class Ila histone deacetylases. *FEBS Lett.* **584**, 1103–1110 <https://doi.org/10.1016/j.febslet.2010.02.057>
- 41 Xie, X.L., Nie, X., Wu, J., Zhang, F., Zhao, L.L., Lin, Y.L. et al. (2015) Smooth muscle 22 α facilitates angiotensin II-induced signaling and vascular contraction. *J. Mol. Med. (Berl)* **93**, 547–558 <https://doi.org/10.1007/s00109-014-1240-4>
- 42 Zhang, R., Shi, L., Zhou, L., Zhang, G., Wu, X., Shao, F. et al. (2014) Transgelin as a therapeutic target to prevent hypoxic pulmonary hypertension. *Am. J. Physiol. Lung Cell. Mol. Physiol.* **306**, L574–L583 <https://doi.org/10.1152/ajplung.00327.2013>
- 43 Falk, M.D., Liu, W., Bolanos, B., Unsal-Kacmaz, K., Klippel, A., Grant, S. et al. (2014) Enzyme kinetics and distinct modulation of the protein kinase N family of kinases by lipid activators and small molecule inhibitors. *Biosci Rep.* **34**, e00097 <https://doi.org/10.1042/BSR20140010>
- 44 Zhao, J., Zhou, D., Guo, J., Ren, Z., Zhou, L., Wang, S. et al. (2006) Effect of fasudil hydrochloride, a protein kinase inhibitor, on cerebral vasospasm and delayed cerebral ischemic symptoms after aneurysmal subarachnoid hemorrhage. *Neurol. Med. Chir. (Tokyo)* **46**, 421–428 <https://doi.org/10.2176/nmc.46.421>
- 45 Aleku, M., Schulz, P., Keil, O., Santel, A., Schaeper, U., Dieckhoff, B. et al. (2008) Atu027, a liposomal small interfering RNA formulation targeting protein kinase N3, inhibits cancer progression. *Cancer Res.* **68**, 9788–9798 <https://doi.org/10.1158/0008-5472.CAN-08-2428>
- 46 Santel, A., Aleku, M., Röder, N., Möpert, K., Durieux, B., Janke, O. et al. (2010) Atu027 prevents pulmonary metastasis in experimental and spontaneous mouse metastasis models. *Clin. Cancer Res.* **16**, 5469–5480 <https://doi.org/10.1158/1078-0432.CCR-10-1994>
- 47 Schultheis, B., Strumberg, D., Santel, A., Vank, C., Gebhardt, F., Keil, O. et al. (2014) First-in-human phase I study of the liposomal RNA interference therapeutic Atu027 in patients with advanced solid tumors. *J. Clin. Oncol.* **32**, 4141–4148 <https://doi.org/10.1200/JCO.2013.55.0376>
- 48 Shiga, K., Takayama, K., Futaki, S., Hutt, J.E., Cantley, L.C., Ueki, K. et al. (2009) Development of an intracellularly acting inhibitory peptide selective for PKN. *Biochem. J.* **425**, 445–453 <https://doi.org/10.1042/BJ20090380>
- 49 Bauer, A.F., Sonzogni, S., Meyer, L., Zeuzem, S., Piiper, A., Biondi, R.M. et al. (2012) Regulation of protein kinase C-related protein kinase 2 (PRK2) by an intermolecular PRK2-PRK2 interaction mediated by its N-terminal domain. *J. Biol. Chem.* **287**, 20590–20602 <https://doi.org/10.1074/jbc.M111.327437>
- 50 Stuckey, D.J., Carr, C.A., Tyler, D.J., Aasum, E. and Clarke, K. (2008) Novel MRI method to detect altered left ventricular ejection and filling patterns in rodent models of disease. *Magn. Reson. Med.* **60**, 582–587 <https://doi.org/10.1002/mrm.21677>
- 51 Geyer, S.H., Maurer-Gesek, B., Reissig, L.F. and Wening, W.J. (2017) High-resolution episcopic microscopy (HREM): simple and robust protocols for processing and visualizing organic materials. *J. Vis. Exp.* **125**, 56071 <https://doi.org/10.3791/56071>
- 52 Mohun, T.J. and Wening, W.J. (2012) Embedding embryos for high-resolution episcopic microscopy (HREM). *Cold Spring Harb. Protoc.* **2012**, 678–680 <https://doi.org/10.1101/pdb.prot069583>
- 53 Wening, W.J., Maurer-Gesek, B., Reissig, L.F., Prin, F., Wilson, R., Galli, A. et al. (2018) Visualising the cardiovascular system of embryos of biomedical model organisms with high resolution episcopic microscopy (HREM). *J. Cardiovasc. Dev. Dis.* **5**, 58 <https://doi.org/10.3390/jcdd5040058>

- 54 Ewels, P.A., Peltzer, A., Fillinger, S., Patel, H., Alneberg, J., Wilm, A. et al. (2020) The nf-core framework for community-curated bioinformatics pipelines. *Nat. Biotechnol.* **38**, 276–278 <https://doi.org/10.1038/s41587-020-0439-x>
- 55 Dobin, A., Davis, C.A., Schlesinger, F., Drenkow, J., Zaleski, C., Jha, S. et al. (2013) STAR: ultrafast universal RNA-seq aligner. *Bioinformatics* **29**, 15–21 <https://doi.org/10.1093/bioinformatics/bts635>
- 56 Li, B. and Dewey, C.N. (2011) RSEM: accurate transcript quantification from RNA-Seq data with or without a reference genome. *BMC Bioinformatics* **12**, 323 <https://doi.org/10.1186/1471-2105-12-323>
- 57 Sonesson, C., Love, M.I. and Robinson, M.D. (2015) Differential analyses for RNA-seq: transcript-level estimates improve gene-level inferences. *F1000Res.* **4**, 1521 <https://doi.org/10.12688/f1000research.7563.1>
- 58 Love, M.I., Huber, W. and Anders, S. (2014) Moderated estimation of fold change and dispersion for RNA-seq data with DESeq2. *Genome Biol.* **15**, 550 <https://doi.org/10.1186/s13059-014-0550-8>
- 59 Marshall, A.K., Barrett, O.P.T., Cullingford, T.E., Shanmugasundram, A., Sugden, P.H. and Clerk, A. (2010) ERK1/2 signaling dominates over RhoA signaling in regulating early changes in RNA expression induced by endothelin-1 in neonatal rat cardiomyocytes. *PLoS One* **5**, e10027 <https://doi.org/10.1371/journal.pone.0010027>